Single spin detection

Maksym Sladkov

Supervisor: Prof. Dr. Bart van Wees

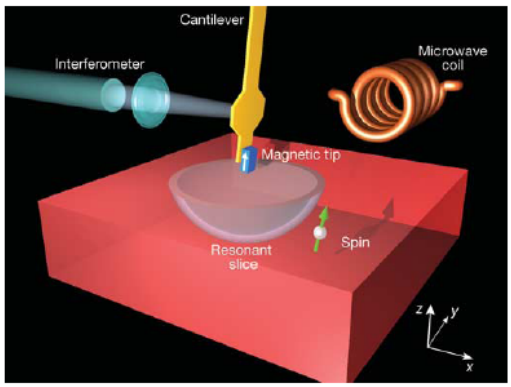

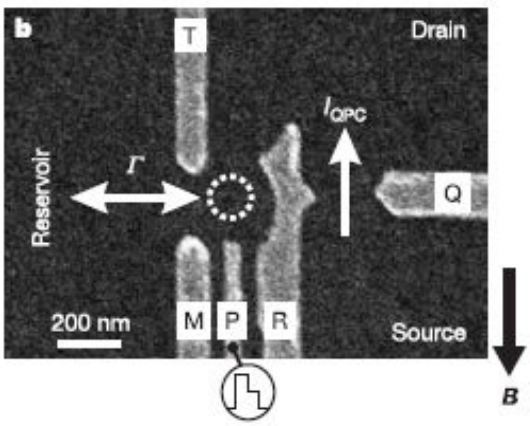

Contents

1. Introduction **3**

2. Electron spin **3**
2.1. What is spin? 3
2.2. Spin in magnetic field 4
2.3. Adiabatic inversion 5
2.4. Zeeman effect 5
2.5. Spin relaxation 5
2.6. Rabi oscillations 6
2.7. Spin blockade 6

3. Field-effect transistor (FET) technique **7**
3.1 Basic idea 7
3.2. Charged electron states of paramagnetic trap 8
3.3. I-V characteristics of the FET with paramagnetic trap. 9
3.4. ESR detection. 10

4. Measuring of single electron spin in QD using three Quantum Point Contacts (QPC). **11**
4.1. Basic idea. 11
4.2. Measurements procedure 12
4.3. Accuracy and fidelity. 14

5. Single spin detection by Magnetic Resonance Force Microscopy (MRFM). **15**
5.1. Basic idea. 16
5.2. The basic principles of OSCAR and *i*-OSCAR techniques. 17
5.3. MRFM experiment 18
5.4. Applications and perspectives. 20

References **21**

1. Introduction

The growing interest in single spin detection is associated with a possible application in a solid state quantum computing [1], new 3-D imaging techniques for molecular structure determination and, indeed, deeper understanding of quantum mechanical processes on a single electron scale [2].

Thus, the spin based quantum computer suggests that using both the spin degree of freedom of the electron as a carrier of classical information (bits) [3], and the idea of using unique properties of quantum mechanics for performing computations leads to a true quantum computer. The using of spin degree of freedom is not only preferably due to the quantum mechanical nature of the spin but also is the requirement of the time, when the size of distinguishable elements on the computer chip approaches atomic scale and quantum effects dictate device behavior.

The 3-D imaging of the biological structures is possible now through the labeling protein and DNA by attaching compounds with unpaired electrons [4]. More generally, the three-dimensional structure of any self-assembling protein/DNA complex might be studied by spin labeling its individual components. The spin labeled components is detected by Magnetic Resonance Imaging (MRI) and Magnetic Resonance Force Microscopy (MRFM) techniques.

In general, the idea of single spin detection can be formulated in two ways: detection of signals from single spin by measuring single Electron Spin Resonance (ESR) that can be used for imaging purposes, and detection of the single spin quantum state, namely single spin manipulation, that is crucial for quantum computing.

While the detection of the single spin through use of ESR was not possible for a long time due to the requirement of large number of spins ($10^8 - 10^{10}$) in order to make ESR signal measurable on the background of noise, the detection of the spin state is even more challenging task due to the collapsing of spin wavefunction by the perturbation potential [5]. Nevertheless, during last few year different experiments on spin detection were reported. Sensing of single spins has been achieved through use of optical [6, 7], STM [8], electrical [9, 10] and MRFM [11] sensing techniques.

In this article the description of electrical and MRFM techniques are presented. Chapter 2 is devoted to introduction in the nature of spin, and to the properties that were used for spin detection in techniques under the interest. Chapter 3 describes experiment on detection of ESR resonance of single paramagnetic trap in the gate region of field effect transistor. Chapter 4 is about the single spin quantum state detection in the QD that is the prominent step toward the spin quantum computer and MRFM technique with single spin sensitivity is described in Chapter 5.

2. Electron spin

2.1. What is spin?

Spin is a fundamental property of all elementary particles in general and electrons in particular. Classically it can be viewed as the intrinsic angular momentum but due to its pure quantum mechanical nature only two electron spin states along external magnetic field can be measured: parallel or anti-parallel to the field. There is a magnetic moment connected to the spin that is indeed pointed opposite to the angular moment direction due to the negative charge carried by electron. It's conventional to talk about magnetic moment direction rather than about angular moment when the spin orientation is considered.

The magnetic moment connected to the spin possess pure quantum mechanical properties. This means that the different components of magnetic moment vector cannot be measured at the same time due to the fact that referred angular momentum operators do not commute.

The spin of an electron is characterized by a spin quantum number s, which for electron takes the value of 1/2. The value of any component of the angular momentum can only take one of 2s + 1 possible values, namely: $s\hbar$, $(s - 1)\hbar$,…, $-s\hbar$. The component of spin angular

momentum is written $m_s\hbar$. For an electron, with $s = 1/2$, this means that there are only two possible values of $m_s = \pm 1/2$. The component of angular momentum along a particular axis is then $\hbar/2$ or $-\hbar/2$. The magnitude of the spin angular momentum for an electron is $\sqrt{s(s+1)}\hbar = \sqrt{3}\hbar/2$. The corresponding magnetic moment of the electron along the z-axis is $\mp m_s \mu_B$.

2.2. Spin in magnetic field

As far as spin can be considered as the intrinsic angular moment of electron and there is a magnetic moment carried by the spin, the electron will have the tendency to precess in the presence of magnetic field.

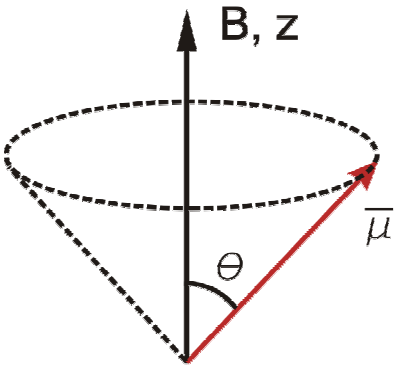

Fig. 2.1 A magnetic moment μ in a magnetic field B precesses around the magnetic field at the Larmor precession frequency, γB, where γ is the gyromagnetic ratio. The magnetic field B lies along the z-axis and the magnetic moment initially in the xz-plane at an angle θ to B. The magnetic moment precesses around a cone of semi-angle θ

Interaction of magnetic field with magnetic moment will exert a torque on the spin resulting in an angular moment precession around the field direction with a Larmor frequency $\omega_L = \gamma B$, where γ is a gyromagnetic ratio that connects the angular and the magnetic moments of the spin trough the relation $\vec{\mu} = -\gamma\vec{L}$. Under this motion spin will draw a cone, where cone angle will depend on the strength of the applied field (Fig. 2.1).

The situation is becoming more interesting in the presence of alternating time-periodic magnetic field. It's useful to break the periodic time dependent field into two rotating components, each of the same amplitude H_1, but one is rotating clockwise while another counterclockwise. It's shown everywhere [12] that near the resonance counterrotating component can be neglected.

Now, the equation of motion must be written with including both, static and periodic magnetic fields resulting in equation of motion for magnetic moment:

$$\frac{d\vec{\mu}}{dt} = \vec{\mu} \times \gamma\left[\vec{H}_0 + \vec{H}_1(t)\right]$$

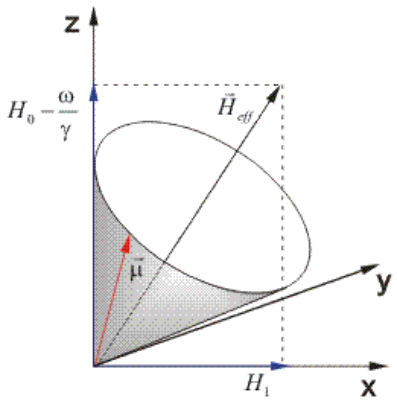

Fig. 2.2 Motion of the magnetic moment μ in the rotating coordinate system. Spin is precessing around the vector of effective field that lies in the xz-plane. z-component of effective field is frequency dependent and vanishes under the resonance condition that results in magnetic moment motion in zy-plane.

The time dependence can be eliminated by using a coordinate system that rotates with a frequency of periodic field yielding in the equation of motion in rotating frame:

$$\frac{d\vec{\mu}}{dt} = \vec{\mu} \times \gamma\left[\left(\vec{H}_0 - \frac{\omega}{\gamma}\right)\hat{z} + \vec{H}_1\hat{x}\right] = \vec{\mu} \times \vec{H}_{eff}$$

It's easy to see that in rotating frame the spin is precessing around the effective field $\vec{H}_{eff}$ (Fig. 2.2). The direction of effective field turns out to be frequency dependent that gives three different types of spin motion. When $\gamma H_0 > \omega$, it results in spin precession around the effective field with positive z-

component, when $\gamma H_0 < \omega$, it changes the sign of the *z*-component of effective field. The third case is the most interesting because it corresponds to the spin resonance. When $\gamma H_0 = \omega$, the *z*-component of the effective field is vanishing and leads to the precession of the magnetic moment in the *yz*-plane. It's important to note that during the resonance, the magnetic moment always remains perpendicular to the direction of $\vec{H}_1$. Now the idea of spin resonance is becoming clearer. During the precession motion spin spends half a period being oriented opposite to the static field that is energetically unfavorable. The required energy spin is absorbing from the alternating field.

2.3. Adiabatic inversion

It can be proven [12] that if electron is in a rotating magnetic field, and the frequency of induced precession is larger then the frequency of rotation, namely $\gamma H_0 >> \omega$ than the magnetic moment will turn with H_0, always remaining aligned along $\boldsymbol{H_0}$.

The fact that magnetization follows the direction of the magnetic field when the field changes direction sufficiently slowly is described by the term *adiabatic*.

One important sequence of adiabatic process can be seen from the next experiment. If there are both static and alternate magnetic fields presented and the system is below the resonance than magnetization is nearly parallel to the effective filed in rotating frame. As one approaches resonance, both magnitude and direction of the effective field change, but if resonance is approached sufficiently slowly, magnetization will remain parallel to the effective field in rotating frame. Thus, exactly at resonance, the magnetization will lie along $\boldsymbol{H_1}$, making 90° degree with $\boldsymbol{H_0}$,

If one will to continue on through the resonance, the magnetization would end up by pointing in the negative z-direction. This technique of inverting magnetization is called *adiabatic inversion*. The particular application for the spin detection will be described in Ch.5.

2.4. Zeeman effect

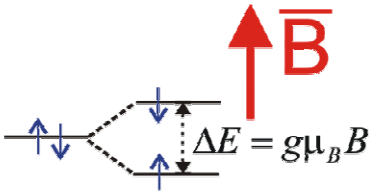

Fig 2.3 Zeeman splitting of discrete level in presence of magnetic field. The g-factor in the expression for the splitting energy is equal 2 for noninteracting spin.

If electron is spatially confined, like in atom or in quantum dot, its energy spectra is discrete and the population of energy levels obey the Pauli principle, namely every level can be only doubly occupied with spin-up and spin-down electron.

In the presence of magnetic field spin-up and spin-down electrons have a different energy due to the energy level splitting, known as Zeeman splitting (Fig. 2.3). The resulting energy separation between the two levels is given by $\Delta E = g\mu_B B$, where g is gyromagnetic, or Lande factor that includes the fact, that not only spin but also angular orbital moment contribute to the interaction with magnetic field. For single spin the g-factor is equal 2, but when spin-orbital coupling or interaction with conductive electrons is presented this value can be different.

2.5. Spin relaxation

The motion of noninteracting spins has in common a periodic motion of the magnetization in the rotating frame. In general, the magnetization that is precessing around $\boldsymbol{H_1}$ in the rotating frame, becoming alternately parallel and antiparallel to the direction of the static field in laboratory system, resulting in non-equilibrium population of spin-up and spin-down states. However, the energy that must be supplied to turn spins from parallel to antiparallel to the static field is recovered when the spins return to being parallel to the static field. Thus, there is no cumulative absorption over long times but rather an alternate absorption and recovery.

When the dissipative processes are included, then it's convenient to describe system through the Bloch equations for spin population, via introducing two different characteristic relaxation times. First, is the population relaxation time T_1 (also called longitudinal) that represents the "lifetime" of the first order rate process that returns the magnetization to the Boltzman equilibrium along the $+z$ axis. The processes that contribute to the T_1 are directly leading to the energy dissipation. Second is the spin-spin relaxation (transverse) time T_2. This time represents the lifetime of the signal in the transverse plane (xy-plane) and is not connected with energy dissipation but rather with a phase decoherence. Presence of relaxation leads to the broadening of resonance line. In liquids T_1 and T_2 are of the same order, while in solids only T_2 is determining the linewidth. Experimental measurements of these times are of great interest especially with connection to single-spin detection that can give deeper understanding of relaxation processes on microscopic level.

2.6. Rabi oscillations

The classical description of spin resonance says that spin is precessing around the $\boldsymbol{H_1}$ field in the rotating frame being always perpendicular to that field. However, quantum mechanical description is considering resonance as the excitation of the system from the ground to excited state, namely to the creation of non-equilibrium population of excited state. At this point one can ask a reasonable question, how does the classical picture with the periodic changing of spin-up and spin-down population finds agreement with the quantum mechanical approach, which results in non-equilibrium population of spin-down state?

The answer lies in effect called the Rabi oscillation. In the damping free systems, the spin resonance does not lead to the stationary non-equilibrium population of spin-down state, but rather to the population oscillation between ground and excited states with a Rabi frequency γH_1, which is in a good agreement with the classical picture that demands spin precession around the $\boldsymbol{H_1}$ field with the same frequency.

In order to see Rabi oscillations in real systems, were the damping processes lead to the non-equilibrium population relaxation, the Rabi frequency must be larger than the typical population relaxation rate T^{-1}, hence the amplitude of the alternating field must be as large as possible. However, the presence of alternating field is changing the spin resonance condition; hence the amplitude of the alternating field must be still less than the magnitude of the static field in order to make perturbation theory be valid.

2.7. Spin blockade

The origin of this name comes from the fact that spin blockade is quite similar to the famous *Coulomb blockade* [13], where electron injection inside a small enough object is depending on the electric charge that object is possessing. Coulomb blockade can be easily observed in electron tunneling experiment from bulk metal (reservoir) into small metallic particle. Tunneling will be possible only when chemical potential of reservoir is matches or higher than chemical potential of small particle that can be achieved by applying an appropriate bias voltage. Electron tunneling leads to increasing of electric charge of particle and hence to the rising of electrostatic energy that can be estimated as energy of charged capacitor. This rising of energy leads to shifting of the chemical potential of particle and, if this change in energy is large enough than the situation, when the tunneling is prevented, is possible.

The idea, that lies in a spin blockade is based on the fact that due to the Pauli exclusion principle every quantum discrete level can be occupied only by two electrons with different orientation of spin – 'up' and 'down' respectively. This means that tunneling into this level will be possible only when level is empty, or half-occupied (one electron occupancy).

The situation is becoming more interesting in the presence of magnetic field that causes Zeeman splitting of level. This splitting leads to the difference in energy, when spin-up state has lower energy than spin-down state. If now the Fermi level of the reservoir lies between Zeeman sublevels, the tunneling will be possible only to the lower energy state with well defined spin orientation – spin-up, and when this state will be occupied tunneling will not be

possible anymore. In a case, when for some reason electron from spin-up state will be excited to the spin-down state (by electron spin resonance e.g.), the tunneling will be possible again. This spin-orientation depending effect can be characterized as *spin blockade*.

3. Field-effect transistor (FET) technique

This technique was successfully realized in 2004 and described in [9]. The importance of this technique is rising from the fact that semiconductor material is used and provides extremely long spin decoherence time [14], that can be used in spin based quantum computer with a single spin as quantum bit (qubit).

3.1 Basic idea

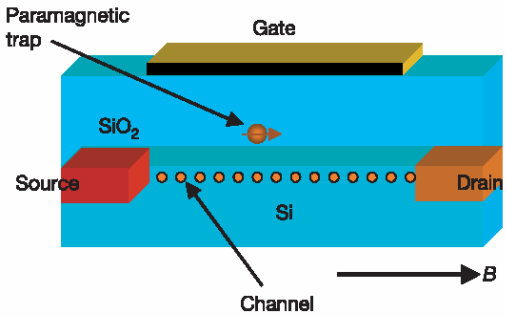

Fig. 3.1 Sketch of n-channel field-effect transistor with a single paramagnetic trap near the SiO2/Si interface

In a field-effect transistor source-drain current is strongly modulated by gate voltage. Roughly speaking, an applied gate voltage leads to induction or depletion of electric charges near the SiO_2/Si interface. This region is usually called channel and there are n- and p-channel FETs can be distinguished, depending on the type of charge carriers that conduct a current. If, for example, one considers n-channel FET, then an applied positive gate voltage (V_g) will lead to inducing of electrons near the SiO_2/Si interface, or in other words to broadening of conducting channel, that results in increasing of source-drain current. On the other side, negative V_g leads to the depletion and for some value even for collapsing of conducting channel that physically means a situation when there are no free charge carriers in the channel and correspond to the so-called pinch-off gate voltage. When there is a defect present at the SiO_2/Si interface, than it behaves like a charge trap and modulates, in principle, in arbitrary way, the effective gate voltage, that channel feels. This leads, in turn, to the modulation of source-drain current.

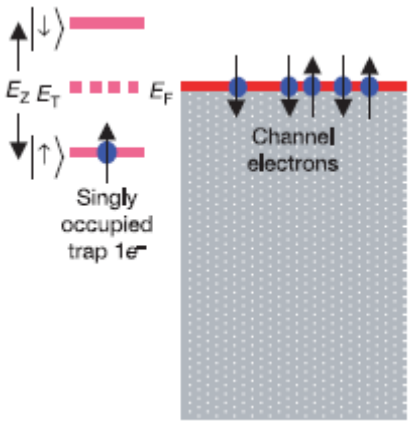

Fig. 3.2 Single occupied paramagnetic trap. Fermi level of the channel lies between Zeeman levels of trap. Further tunnelling from channel to the trap is prevented by spin blockade.

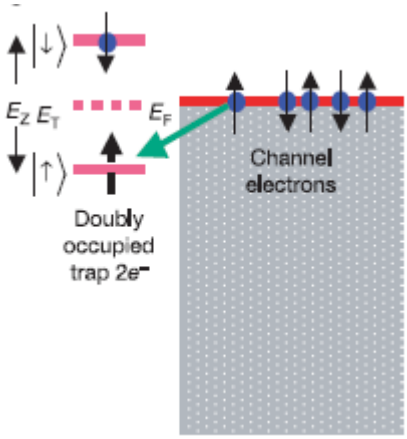

Fig. 3.3 Double occupied trap. Electron are excited to the upper Zeeman level by ESR, that results in releasing of spin blockade and allows tunneling of second electron to the trap.

When the charge trap is a single structural paramagnetic defect [15] within a tunneling distance of the channel and with a charging energy close to the Fermi energy, then spin blockade effects can be expected in the behavior of this trap resulting in two discrete source-drain current values due to the two possible charged states of the paramagnetic trap. These

two states of trap correspond to different spin orientation of trapped electrons. Thus, the spin orientation is converted into the trap charge that can be detected as changes in the source-drain current.

3.2. Charged electron states of paramagnetic trap

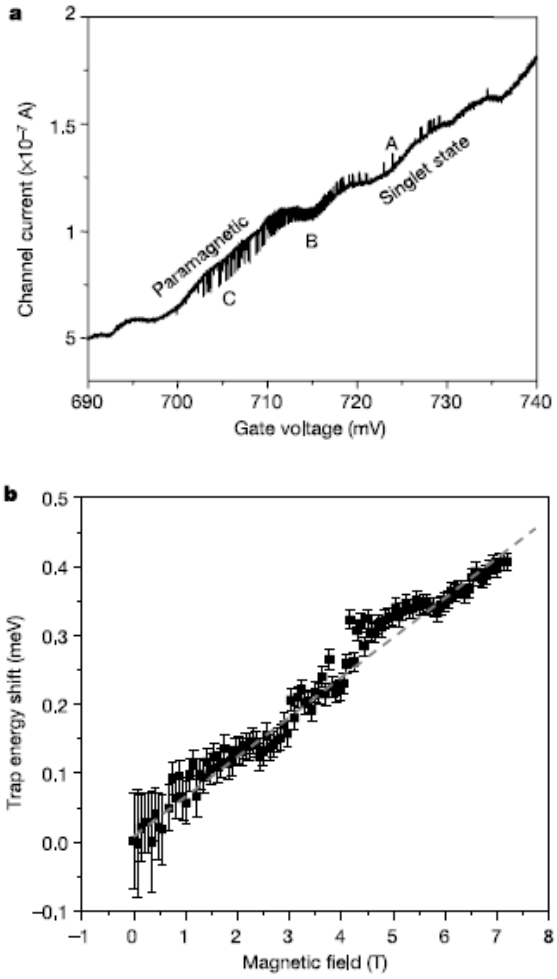

Fig. 3.4 **a.** I_{sd} vs V_g for n-channel FET with a paramagnetic trap near the SiO_2/Si interface. Stochastic behavior of current near the point B corresponds to the gate voltage, when probability of trap to be occupied is near the 50%. Regions near the points A and C correspond to filled and empty trap respectively. **b.** Trap energy dependence on the applied magnetic field. The position of trap energy is detected by changing gate voltage in order to find a region with the most stochastic behavior of current, that indeed corresponds to 50% trap occupancy probability, or in other words, to the matching of Fermi level of conducting channel. For every applied magnetic field correspondent gate voltage was found. Rise of energy with increasing of magnetic field shows that spin-down level is sensed rather than spin-up.

A single paramagnetic trap can be occupied by one or two electrons, but with different orientation of spin, namely spin-up and spin-down. When the trap energy is close to the Fermi level of the conducting channel of the FET and the distance is small-enough for tunneling, then different occupancy of the trap will result in different current through the channel. If the probability of electron to tunnel with spin-up and spin-down is equal then the detection of spin state of the trap is not possible.

When the magnetic field is applied it leads to the Zeeman splitting of energy level of the trap, when spin-up level lies lower than spin-down. This situation results in a different tunneling probability for spin-up and spin-down electron.

While the Fermi level of channel lies between two Zeeman levels of trap, only tunneling to the lower (spin-up) level is possible. When this level is occupied then the next tunneling will be prevented by spin blockade and the trap will possess only $1e^-$ charge (Fig. 3.2).

If an electron from lower (spin-up) level will be excited to the upper (spin-down) level, for example by Electron Spin Resonance (ESR), then spin blockade will be released and tunneling of second electron will be possible resulting in $2e^-$ charge of trap (Fig. 3.3).

The changing of trap charge state from $1e^-$ to $2e^-$ also leads to changing the electrostatic energy and to the Coulomb blockade effects. However, this effect can be neglected if the energy of Zeeman splitting is much larger than correspondent Coulomb blockade energy.

3.3. I-V characteristics of the FET with paramagnetic trap.

The measurements were performed on n-channel Si transistor near the pinch-off region, where the channel size is roughly 300 nm wide and 240 nm long. The signature of a single trap state is shown on Fig. 3.4.**a.** The source-drain current vs. gate voltage without magnetic field being applied shows a monotonic law with well defined stochastic behavior for the certain range of voltage. This stochastic behavior corresponds to the capture and emission of the electron by the trap. A filled trap implies electrostatic repulsion that diminishes the channel current. At high gate voltage (near the point A), the Fermi level of the channel lies well above the trap level and the trap is always occupied resulting in repealing of channel electrons, and hence to less current to flow. For the low gate voltages (below point C), the Fermi level is far below the trap level, and the trap is always empty and does not influence electrons in channel. When the Fermi level of channel is close to the trap level (near the point B), the probability of the trap to be filled is approximately 50% resulting in stochastic behavior of source-drain current, namely jumping between high and low current state, induced by empty and occupied trap respectively. Thus, the source-drain current senses the charge state of the trap.

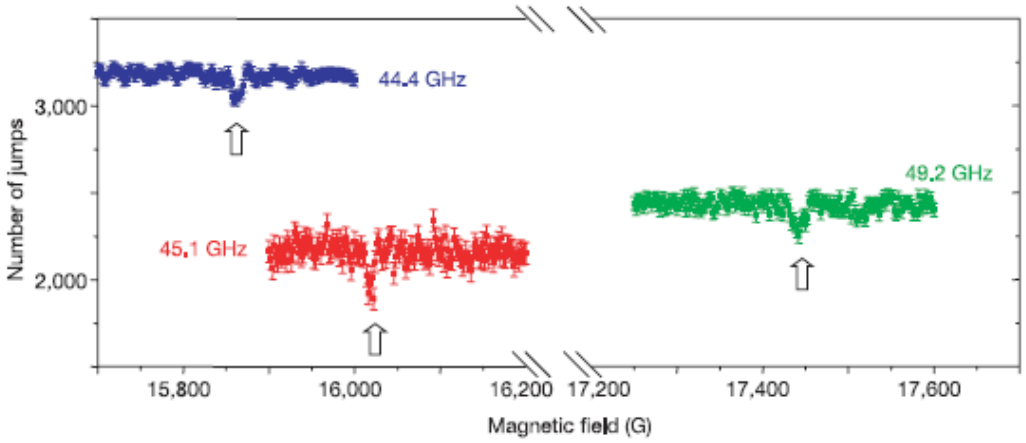

Fig. 3.5 The single electron ESR signal. Number of jumps ($1e^-$ to $2e^-$ transitions), versus magnetic field for a three fixed microwave frequencies. The peak represents electron spin resonance.

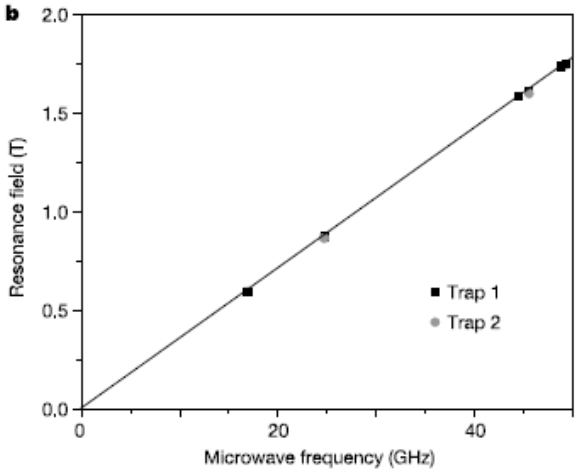

Fig. 3.6 The linear relationship of resonant magnetic field versus microwave frequency indicated a g-factor of 2.02 ± 0.015.

The presence of the magnetic field leads to trap level splitting into the two Zeeman levels. The energy separation between two levels is strongly dependent on the strength of the applied field. Increasing the field leads to the larger Zeeman energy splitting. By tuning the gate voltage the situation when the stochastic behavior of the source-drain current will be the most significant can be found. This corresponds to the situation when the Fermi level and the trap energy level are equal. For every applied magnetic field the correspondent gate voltage can be found. From obtained data the trap energy shift versus applied magnetic field can plotted (Fig. 3.4).

It is obvious, that our current detection technique allows sensing only one of the Zeeman sublevels of the trap level, and hence it can be either spin-up level that corresponds to changing of trap charge state from $0e^-$ to $1e^-$ or spin-down state that corresponds to $1e^-$ to $2e^-$ transition. The fact that energy level is shifting to the higher energy with increasing of magnetic field lets us assume that we indeed deal with $1e^-$ to $2e^-$ transition and with spin-down level respectively.

3.4. ESR detection.

Electron Spin Resonance (ESR) of single spin can be detected using this technique. If in the presence of magnetic field gate voltage is chosen in the way that the Fermi level of channel lies between Zeeman sublevels of the trap, then only tunneling of one electron to the spin-up sublevel is possible, while tunneling of the second electron will be prevented by spin blockade. The source-drain current in the channel will be influenced by $1e^-$ charged trap that corresponds to high level current.

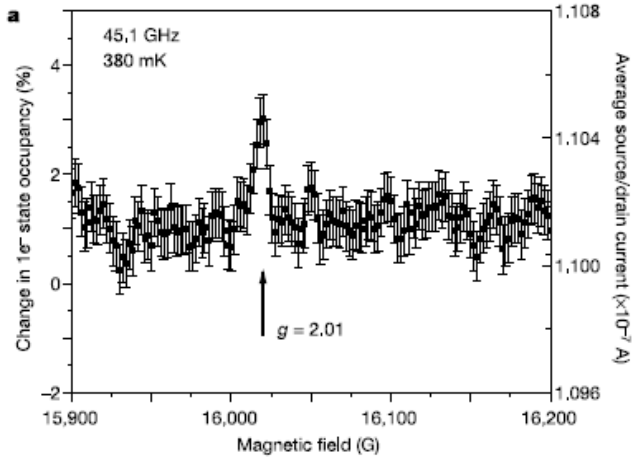

Fig. 3.7 Current trace vs. static magnetic field for high power microwave signal. The induced Rabi oscillation frequency is comparable with a trap tunneling rate that leads to the increasing role of nonlinear effects. This results in the inverting of current trace. The mechanism of this process is not fully clear.

If now, the ESR-microwave signal, with the frequency corresponding to the Larmor frequency of the electron spin is applied, then electron will be excited from spin-up to spin-down Zeeman sublevel, releasing spin blockade and allowing tunneling of the second electron into the trap leading to the change of the trap charge from $1e^-$ to $2e^-$ state. This change in the trap charge state causes decreasing the source-drain current due to the stronger repealing of electrons in channel by charged trap. This corresponds to the low current level.

Fig. 3.5 shows a typical ESR detection trace for the three different frequencies of ESR-microwave signal that indeed correspond to the three different magnetic fields. When the Zeeman splitting of the trap level, namely the Larmor frequency, matches the frequency of the ESR-microwave signal, the resonant spin-up to spin-down transition (spin-flip in other words) is observed as the peak in current, that corresponds to changing between high and low current level. Plotting the magnetic field versus the ESR magnetic resonance frequency (Fig. 3.6) allows determining the g-factor of the paramagnetic centre. For $\hbar\omega_L = g\mu_B B$, the g- factor is found to be 2.02 ± 0.015. The fact that the measured g-factor is larger than 2 indicates that the paramagnetic centre was detected rather than conducting electrons of the n-channel, which always have g < 2 [16]. The observed g-factor is slightly larger than expected [15], which can be caused by some deviation from the ideal local structure of defect, or by slight ferromagnetic ordering of conducting electrons that gives rise to a local field that increases the apparent g-factor of the trap.

The observed transition from high to low current level was only possible within the low microwave power that corresponds to the Rabi frequency oscillation of about $\gamma H_1 \approx 1 kHz$ that is much smaller than electron-trap tunneling rate $\Gamma \approx 20\, kHz$. Thus, nonlinear effects can be neglected. Under these conditions, the full-width half maximum linewidth of the observed resonance is about 5-10 G, which can give us the lower limit of spin-decoherence time $T_2 \approx 0.1$ μs. This time is much less than the typical lifetime for isolated

paramagnetic traps in the SiO_2. This can be caused by the fact that all measurements are done on the operating FET and contribution of the conducting electrons can be significant.

The increase of microwave power leads to the increase of the Rabi oscillation frequency. Thus, when the Rabi frequency is about $\gamma H_1 \approx 10\,kHz$, the Rabi oscillation period starts to be comparable with tunneling time. This results in inversion of the current trace vs. static magnetic field. (Fig. 3.7). This inverting process is not fully clear, and probably is caused by microwave induced changing in tunneling rate or by inverting spin population due to the Rabi oscillation on the typical tunneling time scale.

4. Measuring of single electron spin in QD using three Quantum Point Contacts (QPC).

This technique was reported in 2004 [10] and uses the idea of spin and Coulomb blockade to readout the single electron spin state in a quantum dot (QD) confined in 2DEG via analyses of tunneling current through the QPC.

4.1. Basic idea.

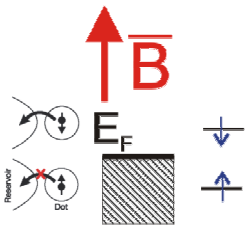

Fig. 4.1 Principle of spin-to-charge conversion. The charge on the quantum dot, Q_{dot}, remains constant if the electron spin is up, whereas a spin-down electron can escape, thereby changing Q_{dot}.

The magnetic field applied to the QD obviously leads to Zeeman splitting of the electron level with different energies for spin-up and spin down electrons. If the QD contains one electron then it can, in principle, have either spin-up or spin-down orientation. Choosing the potential of the dot in the way that only a spin-down electron can tunnel into the bulk metal while a spin-up cannot (Fig. 4.1), namely the Fermi energy of the metal lies between Zeeman sublevels, detection of the spin orientation can be possible, by detecting the charge of the dot. The charge of the dot remains the same if the spin is up, whereas an electron with spin down can escape resulting in a change of the charge of the QD.

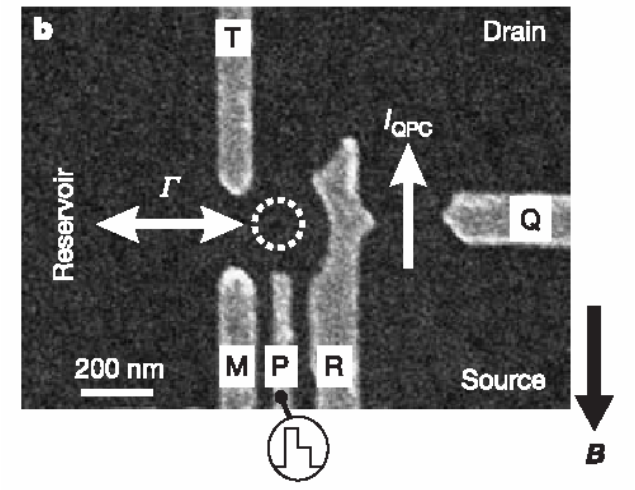

Fig. 4.2 Scanning electron micrograph of a device like the one used in the measurements, showing the metallic gates (T, M, P, R, Q) on the surface of a GaAs/AlGaAs heterostructure containing a two-dimensional electron gas (2DEG) 90 nm below the surface. The electron density is 2.9×10^{15} m^{-2}. By measuring the current through the QPC channel, I_{QPC}, changes in Q_{dot} can be detected that result from electrons tunneling between the dot and the reservoir (with a tunnel rate **Γ**). A magnetic field, ***B***, is applied in the plane of the 2DEG.

All measurements are performed in three steps: (1) emptying the dot, (2) injecting one electron with unknown spin, (3) measuring the spin state.

The measurements were performed using the structure shown in Fig. 4.2, consisting of a quantum dot in close proximity to quantum point contacts (QPC). The QD is formed in the two-dimensional electron gas (2DEG) of a GaAs/AlGaAs heterostructure by applying negative voltages to the metal surface gates M, R and T. This depletes the 2DEG below the gates and creates a potential minimum in the centre, that is, the dot (indicated by a dotted white circle). The potential of gates are chosen in a way, that the

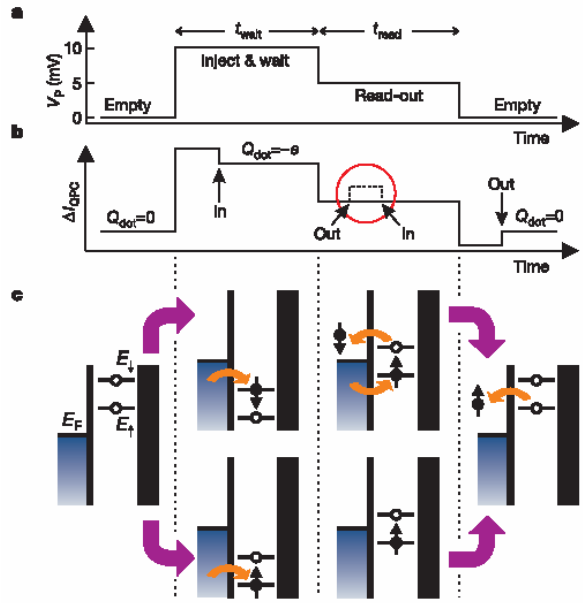

Fig. 4.3 Two-level pulse technique used to inject a single electron and measure its spin orientation. **a**. Shape of the voltage pulse applied to gate P. The pulse level is 10 mV during t_{wait} and 5 mV during t_{read} (which is 0.5 ms for all measurements). **b**. Schematic QPC pulse-response if the injected electron has spin-up (solid line) or spin-down (dotted line; the difference with the solid line is only seen during the read-out stage). Arrows indicate the moment an electron tunnels into or out of the quantum dot. **c**. Schematic energy diagrams for spin-up ($E_\uparrow$) and spin-down ($E_\downarrow$) during the different stages of the pulse. Black vertical lines indicate the tunnel barriers. The tunnel rate between the dot and the reservoir on the left is tuned to a specific value, **Γ**. If the spin is up at the start of the read-out stage, no change in the charge on the dot occurs during t_{read}. In contrast, if the spin is down, the electron can escape and be replaced by a spin-up electron. This charge transition is detected in the QPC current (dotted line inside red circle in **b**)

tunnel barrier between R and T is sufficiently opaque, which prevents the electron tunneling to the drain region on the right, while the tunnel barrier between T and M allows tunneling from dot to the reservoir with tunnel rate $\Gamma \approx (0.05\ \text{ms})^{-1}$. The QPC is created between gates R and Q and is set in the tunneling regime that makes I_{QPC} very sensitive to the electrostatic charge of the QD. Gate P is used for tuning the dot potential (V_P) in order to tune the QD electron energy level with respect to the Fermi level of reservoir. The magnetic field is applied in the plane of 2DEG.

Low V_P corresponds to the empty dot, namely both Zeeman sublevels are above the Fermi level of reservoir. The applied high V_P voltage leads to the lowering of the QD energy level below the Fermi level of the reservoir that allows tunneling of an electron into the QD either with spin up or with spin down. Tunneling of only one electron is possible at this step due to the Coulomb blockade preventing a second electron to tunnel. The P-gate voltage can be also chosen such that the Zeeman spin-down level of the QD will be above the Fermi level and the spin-up level below, that is, corresponds to the situation, that if the electron in the QD has spin-up polarization it will stay on the QD, while an electron with spin-down orientation will tunnel back to the reservoir that will change the electrostatic charge of QD and hence the I_{QPC}. This step is used to detect the orientation of the electron spin in the QD.

4.2. Measurements procedure

As mentioned before, the single-spin measurement technique was tested using a three-stages experiment: (1) emptying the dot, (2) injecting one electron with unknown spin, and (3) measuring the spin state. The different stages are controlled by voltage pulses on gate P (Fig.4.3**a**), which shift the dots energy levels with respect to the Fermi level of reservoir (Fig. 4.3**c**). Changing in I_{QPC} that correspond to different stages is shown on Fig 4.3**b**.

Before the pulse the dot is empty, as both the spin-up and spin-down levels are above the Fermi level of the reservoir, E_F. Then a voltage pulse pulls both levels below E_F. It is now energetically allowed for the electron to tunnel onto the dot, which will happen after a typical time $\sim \Gamma^{-1}$. In general the state of injected electron is unknown. In principal, it can be spin-up, spin-down or the superposition of these two states. Due to the fact that experimental measurements of the spin state can result only in spin-up or spin-down orientation the qualitative

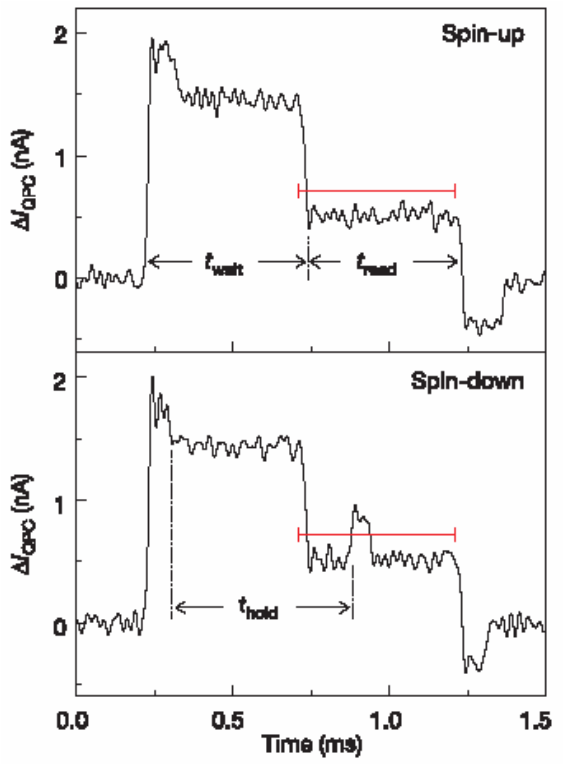

Fig. 4.4 Typical time-resolved measurements of the QPC current in response to a two-pulse. In the top panel, an electron is injected during t_{wait} and is declared 'spin-up' during t_{read}. In the lower panel, the injected electron is declared 'spin-down' by the characteristic step which crosses the threshold (red line) during t_{read}. The total time the electron spends in the dot is defined as t_{hold}.

approach, that after injection the electron can be only spin-up or spin-down, can be used as shown in the lower and upper diagram of Fig. 4.3**c**. During this stage of the pulse, lasting t_{wait}, the electron is trapped on the dot and Coulomb blockade prevents the addition of the second electron. After t_{wait} the pulse is reduced in order to pull the energy levels in the read-out configuration. If the electron spin is up, its energy level is below E_F, so the electron remains on the dot. If the spin is down, its energy level is above the E_F, so the electron tunnels to the reservoir after a typical time $\sim \Gamma_{\downarrow}^{-1}$. Now the Coulomb blockade is lifted and an electron with spin up can tunnel onto the dot within a timescale of $\sim \Gamma_{\uparrow}^{-1}$. After t_{read}, the pulse ends and the dot is empty again.

The expected QPC response, ΔI_{QPC}, consists of two contributions. First, owing to a capacitive coupling between pulse gate and QPC, ΔI_{QPC} will change proportionally to the pulse amplitude. Second, ΔI_{QPC} tracks the charge on the dot. The presence of the negative charge on the dot is decreasing the current, whereas the absence of the charge leads to the current goes up. First change in the charge state of the dot occurs during the injection stage – t_{wait} period, and does not contain any information about the orientation of the electron spin.

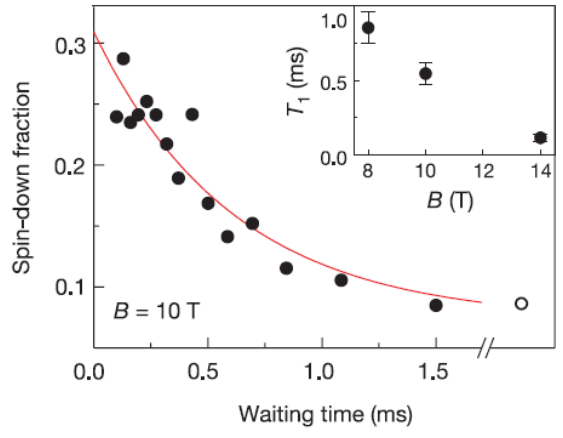

Fig. 4.5 Fraction of traces counted as spin-down versus waiting time, t_{wait}, out of total of 625 traces taken for each waiting time. Solid line: exponential fit to the data. Inset: T_1 versus B.

Second charge changing can occur during the read-out stage. If the spin of the electron is up it will remain on dot and QPC response will consist only from capacitive coupling to the pulse voltage. Otherwise, spin-down electron will tunnel off from the dot, releasing the Coulomb blockade and allowing spin-up electron to tunnel into the dot, that is, indeed results in changing of the charge of the dot that is sensed by ΔI_{QPC} as a step. Measuring whether a step is present or absent during the read-out stage constitutes the spin measurements.

Typical experimental traces of QPC response for both spin-up and spin-down cases are presented in Fig 4.4. It's obvious that the appearance of one of this trace is in principle a random process due to the random orientation of the injected spin. The traces that were obtained fall into two different classes; qualitatively, most of the

traces resemble the one in the top panel of Fig. 4.4 and some resemble the one in the bottom panel (and sometimes, no electron was injected during the injection stage and such cases were ignored). These two typical traces indeed correspond to the signals expected for a spin-up and spin-down. The strong indication of that is the presence of the characteristic step in the spin-down case.

In principle, the spin orientation of the injected electron must be random and the measurements should give the same number over the both types of traces. In reality, the experiment shows that during the read-out stage, the spin-up electron appears to be more often than the spin-down. The explanation of this lies in the fact that after injection electron has to wait some time before the read-out stage will be started and is denoted as t_{wait}. If injected electron had the spin-down polarization, during the time t_{wait}, it could relax to the spin-up (ground) state and this allows the measuring of the single-spin energy relaxation time T_1.

The read-out process does not occur exactly at the beginning of read-out stage due to the stochastic nature of the tunneling process. The time between injection and read-out event is denoted as t_{hold}. As t_{wait} is increased, t_{hold} will vary accordingly to $t_{hold} \approx t_{wait}$.

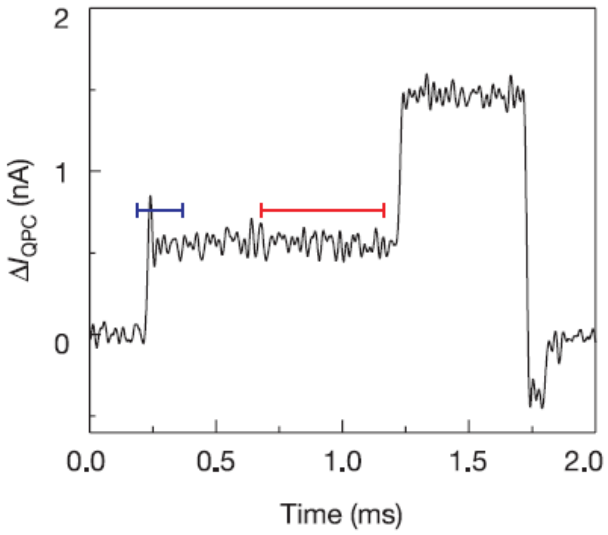

Fig. 4.6 Typical QPC-signal for a 'reversed' pulse, with the same amplitudes as for the direct pulse, but a reversed order of the two stages. The grey threshold is used to obtain open dot in Fig. 4.5, while the black one used in Fig. 4.7.

The measurements were done for 15 different t_{wait}, for each of these times 625 traces were recorded and the fraction of the spin-down traces was counted.

The spin-down fraction versus the waiting time is plotted in Fig. 4.5. Assuming the exponential spin energy relaxation ($\alpha + C \cdot \exp[-t_{wait}/T_1]$) and fitting our experimental data on this low, the average value of T_1 was found to be (0.55 ± 0.07) ms for a magnetic field of 10 T, which is clearly longer than the time needed for the spin measurements (of order $1/\Gamma_\downarrow \approx$ 0.11 ms). Similar experiments at 8 T give $T_1 \approx$ (0.85 ± 0.11) ms and $T_1 \approx$ (0.12 ± 0.03) at 14 T. This is plotted in the inset of Fig. 4.5.

As can be clearly seen, the T_1 is decreasing with increasing the magnetic field. The explanation can come from the fact that spin-flip relaxation is caused by phonons, which have the higher density of states at the higher energies. In fact, in order to test the theoretical prediction that relaxation at high magnetic field is dominated by the spin-orbit interaction [17] with small contribution from the hyperfine interaction with nuclear spins, more measurements must be done.

It's also important to note, that T_1 measurements in principle refer to the entire device under active operation that can strongly influence the measured time.

4.3. Accuracy and fidelity.

During the general description of the performed experiment it was assumed that the tunneling rate for spin-up and spin-down electrons is the same. In reality it is not true [18]. The spin up electron tunneling rate turns out to be larger than the spin down one ($\Gamma_\uparrow > \Gamma_\downarrow$), that results in more probable spin up injection. On the other side, during the read out stage one must be sure, that t_{read} is larger than Γ^{-1}, where $\Gamma = \Gamma_\uparrow + \Gamma_\downarrow$, and this reflects the fact, that the electron with a spin down must tunnel off the dot and after that the spin-up electron will tunnel into the QD resulting in a characteristic step of the I_{QPC} trace.

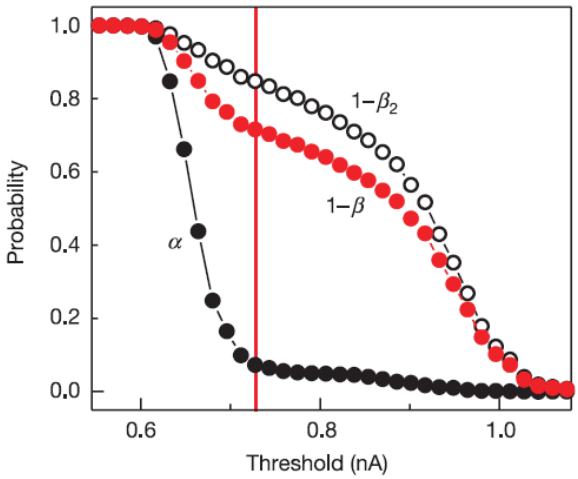

Fig. 4.7 Open squares represent α, obtained from the saturation value of exponential fits in Fig. 4.5 for different values of read-out threshold. Open dots: measured fraction of 'reverse-pulse' traces in which QPC current crosses the injection threshold (black line at 4.6). This fraction approximates $1 - \beta_2$, where β_2 is the probability of identifying a spin-down electron as spin-up owing to the finite bandwidth of the measurement set-up. Closed red dots: total fidelity for the spin-down state, $1 - \beta$, calculated using $\beta_1 = 0.17$. The vertical line indicates the threshold for which the visibility $1 - \alpha - \beta$ (separation between red and black closed dots) is maximal. This threshold value of 0.73 nA is used in the analysis of Fig. 4.4.

For applications in quantum information processing it is important to know the accuracy, or the fidelity, of the single-shot spin read-out. In order to do that, the two parameters will be introduced: α – corresponds to the probability of spin-down detection even if there is a spin-up electron in the QD. This can be possible due to the thermally activated tunneling for example. The second parameter β – corresponds to the opposite process, when the spin-down electron will not be detected, namely will not result in a characteristic step of I_{QPC}.

The parameter α can be found as the saturation value of the exponential fit in Fig. 4.5. that indeed is dependent on the chosen threshold current.

There are two processes that contribute to the β. The first one is due to the spin energy relaxation, and defined as $\beta_1 = 1/(1 + T_1\Gamma_\downarrow)$. This contribution can be calculated by measuring $\Gamma_\downarrow$ from counting the number of spin-down ejection versus the detection time, where the detection time is the time between the start of read-out stage and the moment of peak detection. The found $\Gamma_\downarrow^{-1} = 0.11$ ms yields $\beta_1 = 0.17$. The second contribution to the β can come from the fact, that replacing of the electron in a QD can occur very fast, of the order of 8 μs, and a characteristic step will not be recognizable on the background noise. In order to measure this contribution, a modified 'reversed' pulse was used (Fig. 4.6). For such a pulse, in each trace an electron (with a spin up only) is injected in the dot, so there should always be a step at the start of the pulse. The fraction of traces in which this step is nevertheless missed, namely it was not detected by I_{QPC}, gives us β_2. The fact of the step existence depends on the threshold value for the I_{QPC} that is the free parameter. By plotting $1 - \beta_2$ and α vs. threshold value, the optimal threshold, that is correspond to the maximum visibility, can be found. In presented experiment ($\alpha \approx 0.07$; $\beta_1 \approx 0.17$; $\beta_2 \approx 0.15$) the measurement visibility was found to be 65%. Fig. 4.7.

Significant improvements to the spin detection can be made by lowering the electron temperature that will decrease the probability of quantum fluctuations (smaller α) and by making the charge measurements faster, namely less then the postulated 8 μs (smaller β).

5. Single spin detection by Magnetic Resonance Force Microscopy (MRFM).

Combining three-dimensional MRI with the excellent sensitivity of AFM – MRFM opens the possibility of performing scanning-probe MRI with much improved spatial resolution. Nevertheless, the sensitivity of MRFM for a long time remained to be low for single spin detection. In 2004, by introducing a high gradient magnetic field and a highly sensitive cantilever, Rugar *et al*. succeeded in achieving single spin sensitivity.

5.1. Basic idea.

MRFM is based on the detection of the magnetic force between a ferromagnetic tip and spins in a sample. The main difference between MRFM and conventional Probe Force Microscopy techniques [19] lies in the force detection mechanism that in MRFM is organized by measuring the resonant frequency of the cantilever which indeed depends on the force between the tip and the surface.

The basic elements of the MRFM are shown in Fig.5.1. A small magnetic tip is attached to the vertical cantilever and creates a gradient magnetic field. The cantilever is vibrating on its resonance frequency, and vibrations are detected by the optical interferometer. The resonance frequency, as was mentioned before, is depending on the force between the tip and the surface, and is playing a role as feed-back loop parameter. The change in the resonance frequency represents the tip-surface force.

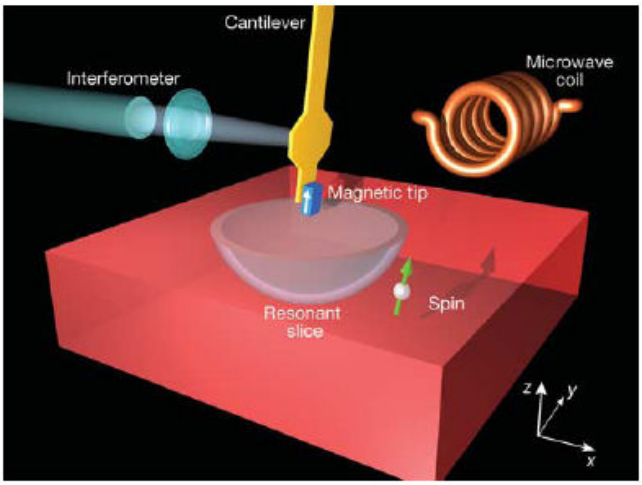

Fig. 5.1 Configuration of the single-spin detection experiment. The resonant slice represents those points in the sample where the field from the magnetic tip (plus an external field) matches the magnetic resonance conditions. When cantilever is vibrate it leads to resonant slice swing back and force through the sample that result in spin flipping and shifting of resonance frequency of cantilever.

Due to its quantum nature, an electron spin can come out only with a spin-up or a spin-down orientation along the chosen direction. Depending on the orientation of the spin with respect to the direction of effective magnetic field (here, and further in this chapter the rotating frame picture is considering) the force between the tip and the surface will be different, namely larger for aligned and smaller for anti-aligned orientation. These two cases will result in either increasing or decreasing the resonance frequency of cantilever. Detection of this cantilever vibration frequency modulation constitutes the spin detection mechanism.

The fundamental challenge in achieving single-spin sensitivity is that the force between a ferromagnetic tip and a spin is in the order of attonewtons, even with a tip field gradient in the gauss per nanometer range. This force is roughly a million times smaller than is typically detected by conventional atomic force microscopy. In order to overcome this problem, resonance force microscopy techniques were used.

To measure a force signal that can be distinguished from the much larger background force fluctuations, that mostly dominated by thermal noise, the "*interrupted* OSCAR" technique was used, where OSCAR stands for oscillating cantilever-driven adiabatic reversal.

5.2. The basic principles of OSCAR and *i*-OSCAR techniques.

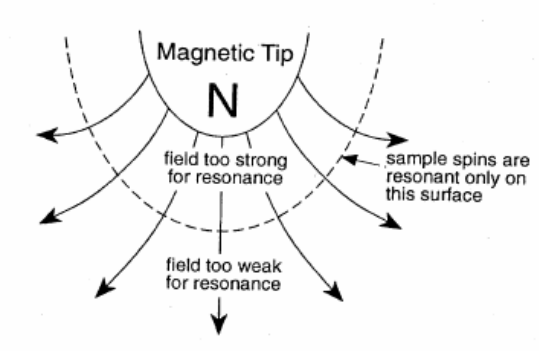

Fig. 5.2 Schematic resonant slice representation. Spin resonance can occur only on the surface depicted as a dotted line.

The main idea of the OSCAR MRFM technique [20] is invented by Dan Rugar and his team. An ultra sensitive micromechanical cantilever (about 100 nm thick) with a ferromagnetic particle (about 1 μm size) attached to the cantilever tip (CT) oscillates near the surface of the sample with a fixed amplitude. The cantilever is oriented perpendicularly to the sample surface and oscillates along the surface.

The magnetic field generated by ferromagnetic tip is not homogeneous, that is why the oscillation of the cantilever leads to a changing magnetic field in the sample. When there is a spin presented in the sample and a microwave signal is applied, the situation when the magnetic field at the spin position will satisfy the spin resonance condition becomes possible. It turns out, that in the case of symmetric (bowl-shape like) tip, the so-called resonance slice is created as shown in Fig. 5.2. The spin precession can occur only when the resonance slice crosses the spin position.

The *z*-component of the spin produces a back magnetic force on the ferromagnetic tip: $F_x = G \cdot \mu_z$, where $G = |\partial B_z / \partial x|$ is the gradient of the magnetic field at the spin position. Since the μ_z is proportional to the magnetic field, namely to the position of cantilever, the magnetic force will be also displacement depended. Thus, the magnetic force influences the effective spring constant of CT and consequently the CT frequency. The CT frequency shift can be measured with high accuracy – this is the main advantage of the OSCAR technique. The direction of the magnetic force acting on CT is opposite to the direction of the spring force. Thus, for the electron spin pointing opposite to the effective field, the CT frequency will decrease. If the electrons spin points in the direction of the effective field, the CT frequency will increase.

If now the location of the spin is out of resonance slice, the spin will precess around the direction of the effective magnetic field in the rotating frame representation. During the periodic motion of the cantilever, the resonance slice will pass through the position of the spin twice during the period of the cantilever motion. If the adiabatic conditions are fulfilled, namely the frequency of the cantilever oscillation is much smaller than the frequency of electron spin resonance, then every passing of the resonance slice through the spin position will lead to a spin flip and a change of sign of the effective field (Ch. 2.3 of this paper). Thus, the relative orientation of the spin with respect to the effective field does not change, resulting in no force change between the tip and the spin. Now, the cantilever resonance frequency depends on the force between the tip and the surface, which is dictated by tip-spin interaction. Depending on the initial orientation of the spin with respect to the cantilever position, namely with respect to the orientation of the effective field, the force between tip and spin can be either positive (parallel orientation) or negative (anti-parallel orientation) resulting in two frequency shifts: $|\delta f_c|$ and $-|\delta f_c|$ respectively. The measurement of the frequency shift constitutes the idea of the OSCAR technique. In reality, the measured signal shows jumps between two frequency levels that are caused by the spin state quantum fluctuations.

In order to increase the sensitivity, the '*interrupted* OSCAR' technique was invented. In this protocol, the *rf* – signal is periodically interrupted for a time equal to the half-period of CT oscillation. This leads to the situation when due to the absence of the resonance slice the spin flip will not occur, while the effective field on the spin will change sign (during the cantilever motion the magnetic field on the spin is changing from the "strong for resonance" to the "weak for resonance" field resulting in a change of sign of the effective magnetic field Fig.5.2) that resulting in a change of sign of the frequency shift. As a result the CT frequency

shift becomes a periodic function of time with twice the interruption period $2T_i$, and the OSCAR signal can be detected at the frequency $1/(2T_i)$ as the frequency modulated signal instead of constant CT frequency shift.

5.3. MRFM experiment

The experiment on the single-spin detection was done on the sample that consist of vitreous silica (Suprasil W2) that was irradiated with a 2-Gy dose of Co^{60} gamma rays. The gamma irradiation produces a low concentration of silicon dangling bonds containing unpaired electron spins known as E' centers [21]. Estimated spin concentration was between 10^{13} and 10^{14} cm^{-3}. The experiments were performed at 1.6 K in a small vacuum chamber that fits within the bore of a superconducting magnet. The low operating temperature minimizes the force noise and reduces the relaxation rate of the spin.

A custom fabricated mass-loaded silicon cantilever [22] with attached 150 nm wide SmCo magnetic tip was used to sense the force from the electron spin. The CT was driven to oscillate with a set amplitude x_{peak} = 16 nm, that corresponds to the fundamental frequency f_c = 5.5 kHz.

The cantilever was scanning along the surface, and single spin detected as the frequency shift of cantilever. In order to detect the small signal from single-spin, the interrupted OSCAR protocol was used, where the microwave field B_1 was turned off for one half of a cantilever cycle every 64 cycles ($f_{int} = f_c/64 \approx 86$ Hz). This leads to the change of sign within the frequency shift of cantilever and therefore to the frequency modulation of the CT oscillation with modulating frequency $f_{sig} = f_{int}/2 \approx 43$ Hz.

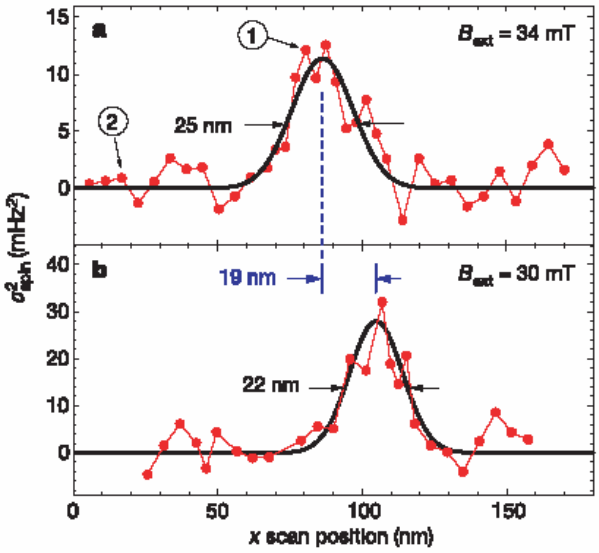

Fig. 5.3 Plots showing the spin signal (time averaged CT frequency shift) as the sample was scanned laterally in the x direction for two values of external field: **a**. B_{ext} = 34 mT, and **b**, B_{ext} = 30 mT. The smooth curves are gaussian fits that serve as guides to the eye. The 19-nm shift in peak position reflects the movement of the resonant slice induced by the 4-mT change in external field. The difference in absolute peak height is primary due to different lock-in amplifier detection bandwidths: 0.18 Hz and 0.59 Hz for **a** and **b**, respectively. Power spectra for the points marked 1 and 2 are shown in Fig. 5.4**a**.

The only first harmonic of the modulated signal was detected that correspond to the quantity $\Delta f(t) = (4/\pi)\cdot|\delta f_c|.A(t)$, where $4/\pi$ comes from first Fourier component of the square wave, δf_c – frequency modulation amplitude and $A(t)$ – is a random telegraph function that takes on values either +1 or -1 and account fact of the possible random spin-flip. For the Poison distributed jumps, $A(t)$ is expected to have a Lorentzian power spectrum.

For the parameters of the current experiment ($G = 2 \times 10^5$ T m^{-1}; k = 0.11 mN m^{-1}; x_{peak} = 16 nm), the expected frequency shift, given by:

$$\delta f_c = \pm \frac{2 f_c G \mu_B}{\pi k x_{peak}}$$

equal to $|\delta f_c| = 3.7 \pm 1.3$ mHz. The estimated uncertainty in $|\delta f_c|$ reflects 20% uncertainties in the calibration of G, k and x_{peak}.

Because the frequency modulation due to the spin is only a few millihertz and the frequency noise of the cantilever due to the thermal motion and tip-sample interaction is relatively large (~ 25 mHz in 1 – Hz bandwidth), the spin-signal to the noise ratio less than 1 and signal cannot be easily extracted. However, if use time

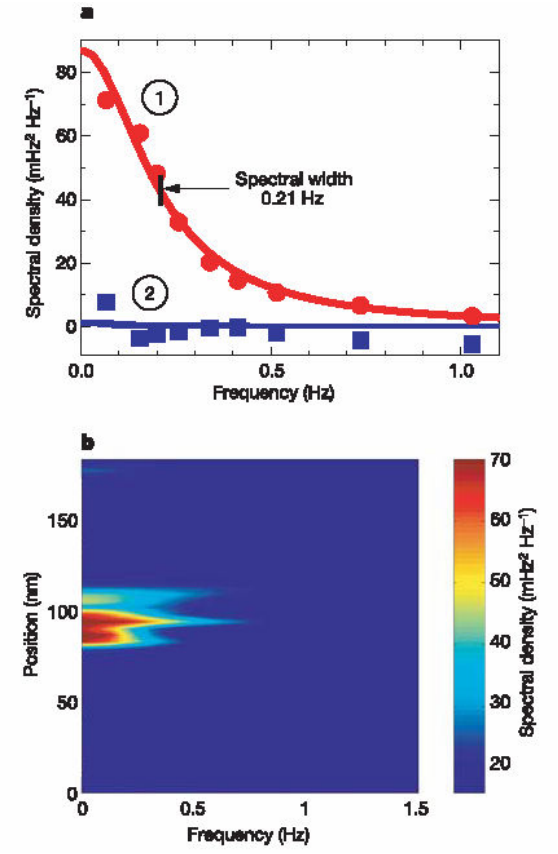

Fig. 5.4 By measuring the spin signal as a function of detection bandwidth, the power spectral density of the spin signal amplitude Δf(t) can be determined. **a**. Spectral density for the two positions indicated in Fig. 5.3. The strong spin signal at position 1 has a narrow spectral width (0.21 Hz), reflecting the long (760 ms) correlation time obtained using iOSCAR spin manipulation. The data are well fitted by a Lorentzian function (solid curve). At position 2, approximately 70 nm away from the position of the spin signal, the spectral density is negligible. **b**. False-color plot showing power spectral density as a function of position. The spin signal is localized both spatially and spectrally. The data were interpolated between discrete measurement positions to create a smooth image. The apparent fine structure in the signal region is probably an artifact of the limited signal-to-noise ration of the original data.

average of square of total signal (time average of the signal obviously gives $\langle \Delta f(t) \rangle = 0$) than for the signal with noise $x + \delta x$:

$$\langle (x+\delta x)^2 \rangle = \langle x^2 \rangle + \langle \delta x^2 \rangle$$

Due to the fact that main contribution to the noise is independent of the spin interaction, namely the noise and the spin-signal are not correlated, noise can be measured and then extracted from the total spin + noise signal.

Fig. 5.3 shows a lateral scan where σ^2_{spin} (frequency shift due to the spin-tip interaction) is plotted as a function of sample position. The scan shows a prominent peak that supposes to be due to the single spin. The peak width is 25 nm, or roughly 1.6 times the cantilever oscillation amplitude. Because the signal-to-noise ratio was so low ($\sigma^2_{spin} / \sigma^2_I \sim 0.06$), considerable averaging was required. The averaging time was 13 h per point, yielding a signal peak that is five standard deviations above the baseline noise.

To confirm that the observed signal is truly due to magnetic resonance, a number of basic tests were performed. As expected for an iOSCAR magnetic resonance signal, the signal disappeared if the microwaves were absent or turned on continuously. The timing of the microwave interruption was also varied. The signal disappeared as expected, when the starting time of the interruption was shifted from the vibration peak to the zero-crossing of the vibration (that is, shifted by one-quarter of a cantilever cycle) and when the interruption duration was a full cantilever cycle instead of one-half cycle.

One key test for magnetic resonance is to observe the field dependence of the spin signal. If the external field is reduced, the resonant slice will shrink in radius, thus shifting the scan position of the signal peak. When B_{ext} was reduced from 34 to 30 mT, the expected peak shift was indeed observed and found to be Δx = 19 nm, as can be seen by comparing the scans in Fig. 5.3. The ratio $\Delta B_{ext} / \Delta x$ suggests that the field gradient G is approximately 2×10^5 T m^{-1} (2 G nm^{-1}).

The conclusion that the signal is due to only one spin is based primarily on the spatial isolation of the spin signal. By design, the spin density of the sample was very low, in the range of 10^{13} to 10^{14} cm^{-3}, giving a mean spacing between spins in the range of 200 to 500 nm. The sparseness of spins implies that, for most sample locations, there is no spin

interacting with the resonance slice. This is why the data in Fig. 5.3 has a zero baseline. To locate a spin signal, the sample was scanned through many independent locations, of the order of 30, before a strong signal from a well-positioned spin was found.

By measuring σ^2_{spin} as a function of detection bandwidth, the power spectral density of the spin signal amplitude Δf(t) can be determined (Fig. 5.4a). As was mentioned before, the only time dependent component of signal Δf(t) coming from a random spin-flip process, that is well described by Lorentzian distribution. That is why the spectra of Δf(t) is well fitted by the Lorentzian function $S(f) = 4\tau_m \left\langle [\Delta f(t)]^2 \right\rangle \Big/ \left[1 + 4\pi^2 \tau_m^2 f^2\right]$. The spectral width of the half-maximum is 0.21 Hz, corresponding to an impressively long τ_m correlation time of 760 ms. The long correlation time implies that the cantilever-driven spin inversions are coherent for thousands of cycles. The false-color image in Fig. 5.4b shows that the spin signal is highly localized both spatially and spectrally.

5.4. Applications and perspectives.

The presented experiment shows that MRFM is now capable of detecting individual electron spins. The most important in this technique is the ability to image the single spin below the surface with nanometer spatial resolution. Spins as deep as 100 nm should be accessible under present operating conditions. It becomes possible due to the few important facts. The inhomogeneous magnetic field forces the spins at the different depth to oscillate at different frequencies; hence a presence of resonance slice provides a spatial resolution. The extremely high sensitivity, of order of 10^{18} newtons, was reached by coherent adding signals together, because the noise contribution, being random, will tend to add to zero. This improvement is limited by the lifetime of the signal coherence; so long spin lifetimes are advantageous. The influence of the thermal fluctuations of the tip was avoided by fabricating mass-loaded cantilever in which the problematic cantilever tip motions are suppressed.

While the square amplitude averaging procedure is used the time consuming is too large, but even a modest increase in the field gradient (for example five times larger) will dramatically speed-up the acquisition time and thereby enable for two- and three- dimensional imaging applications. If the measurements time can be reduced below τ_m, the real-time read-out of the spin quantum state will become possible and probably will allow a wide variety of quantum measurements experiments. The implementation of such kind of experiment can be very useful in understanding the spin wave collapse processes. However, I understand that this statement cannot be taken as primary goal because the adiabatic motion of the spin is crucial in our experiment and that is why, in the proposed experiment, the speed of measurements cannot be faster than the frequency of the spin resonance.

The further increasing of the spatial resolution will allow using the single-spin MRFM in imaging of the bio-molecules and decreasing the read-out time will lead to the observation of molecular processes *in situ*.

Another very important application of MRFM arises from the idea that the quantum computer uses single spin as natural carrier of information (spin-up or spin-down states corresponds to one qubit). With respect to this field the MRFM can find its application for both the readout of spin quantum states and device characterization.

References

1. Divincenzo D.P. "Quantum computation", *Science* **270**, 255-261 (1995).
2. Sidles *et al*., "Magnetic resonance force microscopy", *Rev. Mod. Phys.* **67** (1), 249-263 (1995).
3. Wolf S.A. *et al*., "Spintronics: A Spin-Based Electronics Vision for the Future", *Science* **294**, 1488 (2001).
4. Robinson B.H. *et al*., "Molecular dynamics in liquids – spin-lattice relaxation of nitroxide spin labels", *Science* **263**, 490-493 (1994).
5. Berman G.P. *et al*., "Single spin measurement and decoherence in magnetic-resonance force microscopy", *Phys. Rev. B* **67**, 094425 (2003).
6. Jelezko F. and Wrachtrup J. "Read-out of single spins by optical spectroscopy", J *Phys. Cond. Matt.* **16**; 30, R1089-R1104 (2004).
7. Gywat O. *et al*., "Optical detection of single-electron spin decoherence in a quantum dot", *Phys. Rev. B* **6**, 205303 (2004).
8. Durkan C. and Welland M.E. "Electronic spin detection in molecules using scanning tunneling microscopy assisted electron-spin resonance", *Appl. Phys. Lett.* **80**, 458-460, (2002).
9. Xiao M. *et al*., "Electrical detection of the spin resonance of a single electron in a silicon field-effect transistor", *Nature* **430**, 6998, 435-439 (2004).
10. Elzermann J.M. *et al*., "Single shot read-out of an individual electron spin in a quantum dot", *Nature* **430**, 6998, 431-435 (2004).
11. Rugar D. *et al*., "Single spin detection by magnetic resonance force microscopy", *Nature* **430**, 6997, 329-332 (2004).
12. Slichter C.P. "Principles of Magnetic Resonance", 3rd edn, (*Springer*, Berlin, 1990).
13. Rong, Z. Y. *et al*., "Scanning tunneling microscope observations of the Coulomb blockade", *Phys. Lett. A*, **146** (5), 281-285 (1990).
14. Tyryshkin A.M., Lyon S.A., Astashkin A.V., *et al.*, *Phys. Rev. B* **68** (19),193207 (2003).
15. Poindexter, E.H. in Semiconductor Interfaces, and Devices (ed. Feng, Z.C.) Ch.10, 229-256 (*Inst. Phys. Publ*., Bristol, Philadelphia, 1993).
16. Wallace, W.J. & Silsbee, R. "Spin resonance of inversion-layer electrons in silicon", *Phys. Rev. B* **44**. 12964-12968 (1991).
17. Khaetskii A.V. & Nazarov Y.V. "Spin-flip transitions between Zeeman sublevels in semiconductor quantum dots", *Phys. Rev. B* **64**, 125316 (2001).
18. Hanson R. *et al*., "Semiconductor few electron quantum dot operated as a bipolar spin filter. Preprint at (*http://xxx.lanl.gov/abs/cond-mat/0311414*)" (2003).
19. Binnig G. *et al*., "True atomic resolution by Atomic Force Microscopy through repulsive and attractive forces", *Science* **260** (5113), 1451-1456 (1993).
20. Berman G.P. *et al*., "Modeling and Simulations of a Single-Spin Measurement using MRFM", *TNANO* **4** (1), 14-20 (2005).
21. Castle J.G. *et al*., "Electron spin-lattice relaxation at defect sites: E' centers in synthetic quartz at 3 kilo-Oersteds", *Phys. Rev.* **130**, 577-588 (1963).
22. Chui B.W. *et al*., "Mass-loaded cantilevers with suppress higher-order modes for magnetic resonance force microscopy.", Technical Digest 12th Int. Conf. on Solid-State Sensors and Actuators (Transducers'03) 1120-1123 (IEEE, Piscataway, 2003).